Phase slips and switching in charge-density-wave transport

M. Inui
Department of Physics, Stanford University, Stanford, California 94305-4060

R. P. Hall
AT&T Bell Laboratories, Murray Hill, New Jersey 07974-2070

S. Doniach
Department of Applied Physics, Stanford University, Stanford, California 94305-9040

A. Zettl
Department of Physics, University of California, Berkeley, California 94720
(Received 11 January 1988)

The dynamics of switching charge-density waves (CDW's) are dramatically different from those of nonswitching CDW's. These differences have not been explained by standard models of CDW transport. Phase slippage and strong pinning have recently been proposed as the mechanisms behind switching. In this paper, we present a systematic study of phase slippage, strong pinning, and switching. We begin by constructing a classical Hamiltonian to describe the dynamics of strongly pinned CDW's. From this phenomenological Hamiltonian, overdamped equations of motion are derived to model phase slippage and amplitude collapse in the CDW order parameter. The effects of applied electric fields are numerically investigated and it is found that the equations qualitatively reproduce the experimental characteristics of switching CDW's. Therefore phase slippage provides a self-consistent explanation for the unique transport properties of switching CDW's.

I. INTRODUCTION

The dynamics of sliding charge-density waves (CDW) have been studied extensively since 1973.[1] A seminal paper by Lee, Rice, and Anderson shows that the normal modes of CDW motion approximately correspond to the phase and amplitude coordinates of the CDW order parameter.[2] The dispersion relation for the amplitude mode is gapped so a finite amount of energy is required to create amplitude excitations. In contrast, the dispersion relation for the phase mode of incommensurate CDW's is linear. A vanishingly small amount of energy is required to generate phase excitations in ideal crystals. However, defects such as impurities and dislocations break the translational invariance of the phase mode in real crystals. Consequently, CDW's have an energetically preferred phase with respect to the defect frame.

Defect pinning introduces a gap into the phase-excitation spectrum, but for weak pinning, phase excitations remain easier to excite than amplitude excitations.[3–5] Accordingly, most models of CDW transport have focused on the dynamics of the CDW phase mode.[6–8] In some situations, however, the CDW amplitude mode is excited even in weakly pinned CDW's. Ong and Maki,[9] and independently, Gor'kov,[10] have pointed out that the CDW amplitude must periodically collapse at contacts where current is injected into a sliding CDW. Recent experiments have shown that CDW amplitude fluctuations can occur even in the bulk of a crystal, away from any current contacts.[11,12]

The most dramatic evidence for bulk-amplitude fluctuations has come from experiments on so-called switching crystals.[13] In switching crystals, CDW's depin abruptly and hysterically as the threshold electric field for CDW motion is exceeded. Local measurements of conductivity on single switching crystals show that CDW's break up into regions of uniform phase velocity.[11] Between these regions, excess CDW current is converted into normal electronic current via CDW amplitude fluctuations at phase-slip centers. Indirect experimental evidence has shown that both switching and phase-slip centers are precipitated by localized strong-pinning centers.[14] The dynamics of switching CDW's are dramatically different from the usual dynamics of smoothly depinning CDW's. Besides abrupt depinning and threshold hysteresis, switching CDW's display period doubling, chaos, and an inductive ac conductivity in the sliding regime.[15,16] Phase-dynamical models have been unable to provide satisfactory explanations of these phenomena.

In this paper, we develop and analyze a phenomenological model of CDW dynamics that includes both phase and amplitude degrees of freedom. Specifically, we introduce a Hamiltonian in which the CDW amplitude is reduced by large amounts of phase polarization and in which the CDW phase elasticity is in turn diminished by any reduction in CDW amplitude. At strong-pinning centers, these two processes reinforce one another and lead to transient collapse of the CDW order parameter. From our Hamiltonian, we derive a set of coupled equations for the CDW amplitude and phase, and numerically study a subset of these equations under combined dc and ac electric fields. This subset of equations not only predicts switching and hysteresis,[17] but also period doubling,

 ©1988 The American Physical Society

chaos, and an inductive sliding ac conductivity. Thus, this paper has two main results. First, we derive a set of equations that model the dynamics of strongly pinned CDW's; and second, we provide a self-consistent explanation of the unusual dynamics associated with switching CDW's.

The remainder of the paper is organized into three sections. In Sec. II we derive our so-called phase-slip equations from a generalization of the Fukuyama-Lee Hamiltonian.[3-5] The phase-slip equations are themselves generalizations of the Sneddon-Cross-Fisher hydrodynamical equations.[7] In Sec. III we analyze the response of the phase-slip equations to external electric fields by numerically integrating a special subset of the equations. In Sec. IV we conclude by comparing our results to experiments on switching CDW's.

II. PHASE-SLIP MODEL

A. Hamiltonian and equations of motion

The order parameter of a CDW may be written as $ue^{i\phi}$ where u specifies the amplitude and ϕ the phase of the lattice distortion associated with a CDW. For small distortions of a CDW from equilibrium, Lee, Rice, and Anderson have shown[2] that the CDW amplitude and phase define approximate normal modes whose respective frequencies Ω_+ and Ω_- are given by

$$\Omega_+^2=\lambda\omega_Q^2+\tfrac{1}{3}c^2k^2 ,$$
$$\Omega_-^2=c^2k^2 .$$

Here k is the distortion wave vector, measured from the Fermi wave vector k_F, λ is the dimensionless electron-phonon coupling constant, and Q is the $2k_F$ wave vector with ω_Q the $2k_F$ phonon frequency. The phase-excitation velocity of c is given by $(\hbar^2k_F^2/m^*)^{1/2}$ where m^*, the effective CDW mass, depends on the CDW amplitude as well as the normal electronic mass. In the amplitude dispersion relation, the first term dominates the second, except at large wave vectors. Therefore the wave-vector dependence of Ω_+ can be neglected for the rest of this discussion.

Fukuyama has shown[3] that, in order to treat phase-excitation dynamics, the phase mode may be regarded as an elastic continuum. For strongly pinned CDW's, the Fukuyama Hamiltonian must be generalized to account for the dynamics of the amplitude mode. An appropriate Hamiltonian is

$$\int dx\,[\mu u_0^2(d\phi/dt)^2+\mu(du/dt)^2 + Y_0^2u_0^2(d\phi/dx)^2+\mu\lambda\omega_Q^2(u-u_0)^2] ,$$

where μ is the ionic mass density and u_0 is the equilibrium value of the CDW amplitude. Young's modulus for the phase mode is given by $Y=\mu c^2$ and Y_0 denotes its equilibrium value. (Henceforth we will drop the subscript on Y_0.) In the Hamiltonian, the (small) electronic contribution to m^* has been neglected.

The CDW phase and amplitude coordinates are mixed by large distortions of the CDW order parameter, because they are not exact normal modes of CDW motion. A coupling term must be introduced in order to produce mixing of the amplitude and phase modes; a particularly simple coupling is obtained by requiring that the phase-mode elasticity depend upon the CDW amplitude:

$$Yu_0^2(d\phi/dx)^2\rightarrow Yu^2(d\phi/dx)^2 .$$

Besides being simple, this coupling possesses a feature which is critical to later results: as the CDW amplitude goes to zero, the elasticity of the phase mode vanishes. We will show below that this feature, which must be found in any amplitude-phase coupling term, leads to the phenomena characteristic of switching CDW conduction. Our generalized Fukuyama Hamiltonian is thus given by[5]

$$H_0=\int dx\left\{u^2\left[\mu\left[\frac{d\phi}{dt}\right]^2+Y\left[\frac{d\phi}{dx}\right]^2\right] +\mu\left[\frac{du}{dt}\right]^2+\mu\lambda\omega_Q^2(u-u_0)^2\right\} . \tag{2.1}$$

We will use standard Fukuyama-Lee-Rice terms to describe the interaction of CDW's with applied electric fields and with lattice defects:[3-5]

$$H_{\rm el}=-\int dx\,(\rho^{\rm eff}neE\phi/Q) ,$$
$$H_{\rm def}=-\int dx\left[\sum_j V_j\rho\delta(x-R_j)\cos(Qx+\phi)\right] , \tag{2.2}$$

where n is the electronic density, E is the applied electric field, ρ is the electronic amplitude of the CDW, $\rho^{\rm eff}$ is an effective, normalized CDW density, and the summation is over all pinning sites R_j, whose respective pinning strengths are denoted by V_j. Both ρ and $\rho^{\rm eff}$ depend on the CDW amplitude u, so both act as dynamical variables in Eqs. (2.2).

CDW phase dynamics are well known to be overdamped.[18] We will assume that CDW amplitude dynamics are also overdamped so that both the CDW phase and amplitude obey relaxational equations of motion:[5]

$$\frac{d\phi}{dt}=-\Gamma_\phi\frac{\delta\mathcal{H}}{\delta\phi} ,$$
$$\frac{d}{dt}\left[\frac{u}{u_0}\right]=-\Gamma_u\frac{\delta\mathcal{H}}{\delta\left[\frac{u}{u_0}\right]} . \tag{2.3}$$

Here Γ_ϕ and Γ_u are damping parameters for the phase and amplitude modes, and $\mathcal{H}$ is the combined Hamiltonian density of Eqs. (2.1) and (2.2).

Several approximations simplify Eqs. (2.3) to a more tractable form. First, the equations may be converted into a discretized form by neglecting variations of the CDW order parameter on length scales shorter than the average defect spacing. We will take our discretized Hamiltonians to be

$$H_0=\sum_j \left[l_j Y u_{j+1} u_j \left[\frac{\phi_{j+1}-\phi_j}{l_j} \right]^2 + \xi\mu\lambda\omega_Q^2 (u-u_0)^2 \right] ,$$
$$H_{\rm el}=-\sum_j l_j' \rho_j^{\rm eff} neE\phi_j/Q , \tag{2.4}$$
$$H_{\rm def}=-\sum_j \rho_j V_j \cos(QR_j+\phi_j) ,$$

where time derivatives have been dropped from H_0 because of the assumption of relaxational dynamics. Here $l_j=R_{j+1}-R_j$, $l_j'=\frac{1}{2}(l_j+l_{j-1})$, ξ is the CDW amplitude coherence length, and ϕ_j, u_j, ρ_j, and $\rho_j^{\rm eff}$ denote respective values of ϕ, u, ρ, and $\rho^{\rm eff}$ at the jth pinning site. The concentration n_D of defect sites is related to the average defect spacing by $n_D^{-1}=\bar{l}_j$. Typically, the amplitude coherence length is much shorter than the average defect spacing: $\xi \ll \bar{l}_j$.

Equations (2.3) are further simplified if the CDW coupling to defects and applied electric fields is independent of the CDW amplitude. Amplitude independence is valid when pinning centers are either very weak ($\rho_j V_j \ll n_D u_0^2 Y$) or very strong ($V_j \gg \xi\mu\lambda\omega_Q^2 u_0^2$). At weak centers, the CDW amplitude remains very close to its equilibrium value because the CDW phase depins before sufficient polarization accumulates to suppress the CDW amplitude. At very strong centers, the opposite limit applies: the CDW phase never depins, at least not until the CDW amplitude has collapsed or has nearly collapsed. Except for these transient, singular moments when $u_j \cong 0$, the large value of V_j at a strong-pinning center completely dominates any variations in ρ_j or $\rho_j^{\rm eff}$. (The transient moments when $u_j \cong 0$ will be dealt with in the next section.) Thus at both very weak and very strong impurity sites, the amplitude dependencies of $H_{\rm el}$ and $H_{\rm def}$ are unimportant. Equations (2.3) may be rewritten as

$$\frac{d\phi}{dt}=-\Gamma_\phi \frac{\delta \mathcal{H}}{\delta\phi} ,$$
$$\frac{d\Delta}{dt}=-\Gamma_u \frac{\delta \mathcal{H}_0}{\delta\Delta} , \tag{2.3'}$$

where Δ is the normalized amplitude (u/u_0). The resulting equations of motion are

$$\dot{\phi}_j=l_j'\Gamma_\phi \rho^{\rm eff} nQE-\Gamma_\phi \rho V_j \sin(QR_j+\phi_j) - 2\Gamma_\phi Y u_0^2 \Delta_j \left[\Delta_{j+1} \left[\frac{\phi_j-\phi_{j+1}}{l_j} \right] + \Delta_{j-1} \left[\frac{\phi_j-\phi_{j-1}}{l_{j-1}} \right] \right] ,$$
$$\dot{\Delta}_j=-2\Gamma_u \xi\mu\lambda\omega_Q^2 u_0^2 (\Delta_j-1) - \Gamma_u Y u_0^2 \left[l_j \Delta_{j+1} \left[\frac{\phi_{j+1}-\phi_j}{l_j} \right]^2 + l_{j-1}\Delta_{j-1} \left[\frac{\phi_j-\phi_{j-1}}{l_{j-1}} \right] \right] , \tag{2.5}$$

where $\rho^{\rm eff}$ and ρ are now regarded as constants.

B. Phase slippage

Equations (2.5) are valid only for $\Delta_j > 0$. The equilibrium value of Δ_j is given by

$$\Delta_j^{(\rm eq)}=1-\frac{1}{2}\frac{Y}{\xi\mu\lambda\omega_Q^2} \left[\Delta_{j+1} \frac{(\phi_{j+1}-\phi_j)^2}{l_j} + \Delta_{j-1} \frac{(\phi_j-\phi_{j-1})^2}{l_{j-1}} \right] .$$

At a strong-pinning center, the phase distortions $|\phi_{j\pm1}-\phi_j|$ can become so large that $\Delta^{(\rm eq)} \le 0$. Vanishing or negative values of $\Delta^{(\rm eq)}$ drive the CDW order parameter $\psi=ue^{i\phi}$ toward collapse. Depending on various relaxation rates, ψ may or may not collapse completely, but the effect on the strongly pinned phase is identical. In the case of near collapse, $H_{\rm def}$ becomes so reduced that the accumulated phase polarization forces the phase to move in the direction of E. Because V_j is large at a strong-pinning site, the accumulated phase polarization is also quite large and the phase velocity tends to be high when $\Delta_j \approx 0$. The phase therefore abruptly advances by about 2π, whereupon the phase polarization is relieved, the amplitude Δ_j regenerates, and the phase again becomes stuck at the strong impurity site.

In the case of complete collapse, the CDW phase becomes indeterminate at the strong-pinning site. It may therefore "slip" so that phase polarization is again relieved and the CDW amplitude regenerates. This process is known as phase slippage in superconductors and superfluids.[19,20] Because of phase pinning, the details of phase slippage are slightly different in CDW's. If the CDW order parameter is viewed as a variable in the complex plane, then the first-order differential equations of (2.3) and (2.5) require that ϕ change by exactly $\pm\pi$ (modulo 2π) when ψ crosses zero; the sign and modulus of the phase change are chosen so that $\Delta^{(\rm eq)}$ becomes equal to its smallest possible positive value. Following a $\pm\pi$ phase change at a strong-pinning center, the potential energy of the CDW is at its maximum value. Because V_j is very large at strong-pinning centers, a $\pm\pi$ phase flip is followed by a quick advance of the CDW phase through an additional factor of π.

Thus for either complete or near-complete collapse of the CDW order parameter, the CDW phase abruptly advances by 2π (modulo 2π) at a strong-pinning site. Since we will be interested in CDW dynamics on much longer time scales, we will call both processes phase slips and will approximate both by instantaneous 2π (modulo 2π) hops of the CDW phase. Our complete equations of motion are therefore Eqs. (2.5) augmented by the condition that ϕ changes by $\pm 2\pi$ (modulo 2π) whenever Δ collapses.

C. Reduced phase-slip equations

We now show how Eqs. (2.5) can produce switching and hysteresis. It is convenient to consider a (one-dimensional) crystal of N weak-pinning centers and im-

pose periodic boundary conditions, so that the crystal may be thought of as a closed loop. Each weak impurity is assumed to be of strength $V_w \ll n_D Y u_0^2/\rho$. Fukuyama and Lee[4] have shown that when N is large enough, the crystal breaks into a series of phase domains whose average length is given by

$$L_0=(\eta\pi\epsilon)^{-2/3}n_D^{-1} ,$$

where η is a constant of order unity, n_D is the (weak-) pinning center concentration, and ϵ is the Fukuyama-Lee pinning parameter:

$$\epsilon=\frac{V_w\rho}{u_0^2 Y n_D} .$$

Since the CDW phase within a domain is nearly rigid, the number of dynamical variables is reduced from N (one for the phase at each pinning site) to $N/n_D L_0$ (one for the phase within each domain).

If the average phase within a weakly pinned domain is $\bar{\phi}$, then the effective pinning within the domain is approximately $\bar{V}\cos(\phi-\bar{\phi})$, where $\bar{V}\sim V_w\rho(n_D L_0)^{1/2}$. If a single, very-strong-pinning center is added to the domain, then we assume that the pinning center has three main effects. First, the entire domain will become strongly pinned, because the average phase within the domain cannot depin until the CDW amplitude at the strong-pinning center has collapsed. Second, the average phase within the strongly pinned domain will shift to the phase ϕ_0 that is preferred at the strong-pinning center. Finally, since the amplitude relaxation rate Γ_u is generally much faster than the phase relaxation rate Γ_ϕ, the strongly pinned domain may respond faster than a weakly pinned domain to applied forces.

We now suppose that a single strong-pinning center is added to our model crystal, say at site $j=M$, and that the total number N of weak-pinning centers is small enough so that just two domains are present in the crystal: a strongly pinned domain centered at $j=M$ and a weakly pinned domain in the rest of the crystal. The phase of the strongly pinned domain will be denoted by ϕ_0 and the phase of the weakly pinned domain by ϕ. The only other dynamical variable in the problem is the CDW amplitude Δ at the strong-pinning center. The phase-slip equations of Eqs. (2.5) are greatly simplified:

$$\frac{1}{\Omega_0}\dot{\phi}=e-\sin\phi-\alpha\Delta(\phi-\phi_0) , \tag{2.6a}$$

$$\frac{1}{\Omega_0}\dot{\Delta}=-\frac{1}{\kappa}\left\{\Delta-\left[1-\left[\frac{\phi-\phi_0}{\theta}\right]^2\right]\right\} , \tag{2.6b}$$

$$\phi_0\rightarrow\begin{cases}\phi_0 & \text{if } \Delta>0\\ \phi_0\pm 2\pi & \text{if } \Delta\le 0 .\end{cases} \tag{2.6c}$$

The phase change in ϕ_0 is chosen to minimize $|\phi-\phi_0|$. Here e represents the external electric field applied to the crystal. The electric field is normalized to the characteristic field of the weakly pinned domain:

$$e=E/E_p ,$$

where

$$E_p=Q\bar{V}/neL_0 .$$

CDW current in these equations is proportional to $\dot{\phi}$, so dc current is proportional to $\langle\dot{\phi}\rangle$ where $\langle\ \rangle$ indicates time averaging.

The reduced phase-slip equations are a generalization of the Grüner-Zawadowski-Chaikin model.[6] The equations were previously written down by Hall *et al.*[17] without derivation. From the present derivation, the phase-slip parameters Ω_0, α, κ, and θ can be related to microscopic quantities:

$$\begin{aligned}&\Omega_0=\Gamma_\phi\bar{V} ,\\ &\alpha=2Yu_0^2/\bar{V}L_0 ,\\ &\kappa=\Gamma_\phi\bar{V}/2\Gamma_u\xi\mu\lambda\omega_Q^2u_0 ,\\ &\theta=(4\xi\mu\lambda\omega_Q^2u_0L_0/Yu_0^2)^{1/2} .\end{aligned} \tag{2.7}$$

The first two parameters, Ω_0 and α, are common to classical models of CDW phase dynamics. The frequency Ω_0 is the so-called "crossover frequency" observed in ac-conductivity experiments on CDW's.[21] This frequency is the characteristic relaxation rate of a weakly pinned domain. For the lower CDW state of $NbSe_3$, Ω_0 is about 100 MHz. The parameter α represents the phase elasticity of a CDW, normalized to the weak impurity pinning potential. The value of α depends on the length scale over which one considers CDW dynamics. On the Fukuyama-Lee-Rice coherence length scale, weak impurity pinning just dominates CDW phase elasticity, so a conventional value of α is 0.2. The remaining two parameters, κ and θ, are new to this model of strongly pinned CDW dynamics. The parameter κ represents the relaxation time of the strongly pinned domain. The parameter θ represents the amount of phase polarization necessary to cause amplitude collapse. No conventional choices exist for κ and θ, and we will treat these parameters as adjustable in order to fit experimental data. We discuss appropriate values of θ and κ in Sec. III.

To show that Eqs. (2.6) can exhibit hysteresis and switching, consider the limit that $\alpha\theta\gg 1$ and $\Omega_0/\kappa\gg 1$. This limit corresponds to an extremely polarizable phase and an extremely fast amplitude relaxation rate. In Eqs. (2.6), the weak-pinning term becomes negligible and the CDW amplitude follows the CDW phase polarization without any lag. The CDW equation of motion simplifies to

$$\begin{aligned}&\dot{\phi}\cong e-\alpha(\phi-\phi_0)\{1-[(\phi-\phi_0)/\theta]^2\} ,\\ &\phi_0\rightarrow\begin{cases}\phi_0 & \text{if } |\phi-\phi_0|<\theta\\ \phi_0\pm 2\pi & \text{otherwise} .\end{cases}\end{aligned} \tag{2.8}$$

The elasticity term $\alpha(\phi-\phi_0)\{1-[(\phi-\phi_0)/\theta]^2\}$ is shown in Fig. 1. As e increases from zero, the CDW does not begin to slide until e exceeds the maximum value of the potential. This maximum sets an *upper threshold field* given by

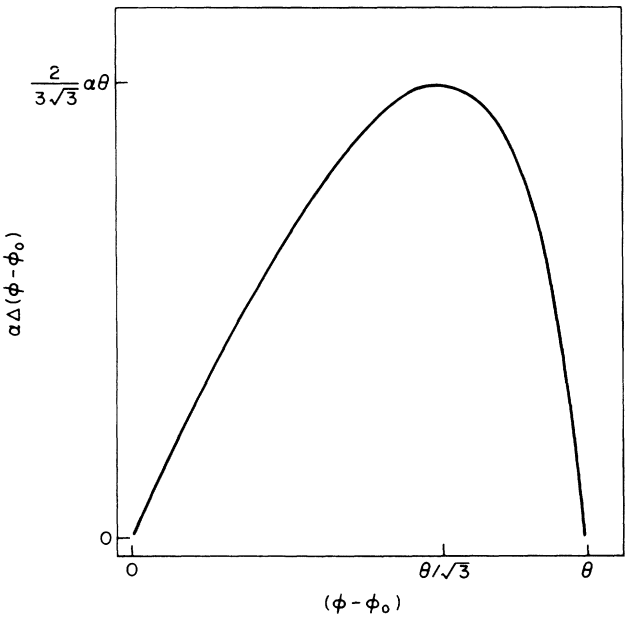

FIG. 1. The phase elasticity $\alpha\Delta(\phi-\phi_0)$ as a function of phase polarization $(\phi-\phi_0)$. The figure applies to the limit that $\Omega_0/\kappa \gg 1$, in which the CDW amplitude becomes a simple function of phase polarization.

$$e_{t2}=\frac{2}{3\sqrt{3}}\alpha\theta \ . \tag{2.9}$$

After the CDW begins to slide, phase slippage keeps $\phi-\phi_0$ in the range $[\theta-2\pi,\theta]$. In this range, the maximum value of the elasticity potential sets a *lower threshold field* given by

$$e_{t1}=\begin{cases} e_{t2} & \text{if } \theta\le(3+\sqrt{3})\pi \\ \alpha\theta\left[1-\dfrac{2\pi}{\theta}\right]\left[1-\left[\dfrac{2\pi}{\theta}\right]^2\right] & \text{otherwise} \ . \end{cases} \tag{2.10}$$

Once e exceeds e_{t2}, the CDW continues to slide as long as e continues to exceed e_{t1}. Therefore when $e_{t1}<e_{t2}$, the CDW stops sliding at an electric field which is lower than the field at which it began sliding, i.e., the motion of the CDW becomes hysteretic. We define a critical polarizability $\theta_H\equiv(3+\sqrt{3})\pi$ which determines the onset of hysteresis: if $\theta>\theta_H$, then $e_{t1}<e_{t2}$ and CDW current is a bistable function of the applied electric field.

In Eqs. (2.8), hysteresis is caused by an abrupt collapse in the elasticity potential once the CDW begins sliding. This collapse also causes switching. Just above the upper threshold field, the minimum instantaneous CDW velocity is $e_{t2}-e_{t1}$, so the time-averaged dc CDW current is larger than this:

$$\langle\dot{\phi}\rangle|_{e=e_{t2}+}>e_{t2}-e_{t1} \ .$$

When $\theta>\theta_H$, dc CDW current jumps from zero to a finite value as e exceeds e_{t2}.

Even away from the limit $\alpha\theta\gg1$ and $\Omega_0/\kappa\gg1$, switching and hysteresis occur in Eqs. (2.6) when θ becomes sufficiently large. As $\alpha\theta$ becomes comparable to 1, the upper and lower threshold fields are given by

$$e_{t2}=\max_{\phi\in[0,\theta]}(\sin\phi+\alpha(\phi-\phi_0)\{1-[(\phi-\phi_0)/\theta]^2\}) \ , \tag{2.11}$$

$$e_{t1}=\max_{\phi\in[\theta-2\pi,\theta]}(\sin\phi+\alpha(\phi-\phi_0)\{1-[(\phi-\phi_0)/\theta]^2\}) \ .$$

As Ω_0/κ becomes comparable to 1, e_{t1} shifts to lower values and the critical polarizability decreases from $(3+\sqrt{3})\pi$. In the limit that $\kappa\to\infty$, both e_{t1} and θ_H go to zero.

D. Inertial effects

In order to gain insight into the dynamics of the phase-slip equations, it is useful to compare the equations to a phase-only model of switching. Switching behavior has been analyzed in terms of the rigid-phase model of Grüner, Zawadowski, and Chaikin.[14–16] The rigid-phase model ignores the existence of phase domains and treats the CDW phase as uniform throughout a crystal.[6] The dimensionless equation of motion is

$$\beta\ddot{\phi}+\dot{\phi}=e-F(\phi) \ , \tag{2.12}$$

where the periodic function $F(\phi)$ represents a pinning force, β is a so-called inertial parameter, and time is measured in units of $(\Omega_0)^{-1}$. When β is small, the phase velocity is a deterministic function of the electric field e and the pinning force F. In this case, the dynamics of Eq. (2.12) are overdamped and the equation does not lead to switching. When $\beta\gtrsim1$, however, the dynamics of (2.12) is underdamped and the equation leads to both switching and hysteresis.[16]

Except for the inertial term $\beta\ddot{\phi}$, the rigid-phase equation is very similar to Eq. (2.6a) of the reduced phase-slip equations. In fact, the equations become identical when $\kappa=0$ and $\theta=2\pi$, because then the elasticity term $\alpha\Delta(\phi-\phi_0)$ in Eq. (2.6a) is a deterministic, periodic function of the phase ϕ. But even when $\kappa>0$ and $\theta\neq2\pi$, the phase-slip and rigid-phase equations are still dynamically equivalent, at least in the following sense: for small ac signals, the ac response of the phase-slip equations maps onto the response of the rigid-phase equation, as long as the inertial parameter β is assumed to be motion dependent.

The response of either the phase-slip or rigid-phase equations is conveniently measured in terms of ac conductivity. For an electric field of the form $e=e_{\rm dc}+e_{\rm ac}\exp(i\Omega t)$, ac conductivity may be defined as

$$\sigma(\Omega)=\tilde{\dot{\phi}}(\Omega)e_{\rm ac} \ ,$$

where $\tilde{\dot{\phi}}(\Omega)$ is the Fourier component of phase velocity at the applied ac frequency. When the CDW in the reduced phase-slip equations is pinned, the CDW phase has an equilibrium value $\phi_{\rm eq}$ that is determined by the dc bias:

$$0=e_{\rm dc}-\sin\phi_{\rm eq}-\alpha\Delta_{\rm eq}(\phi_{\rm eq}-\phi_0) \ .$$

Here the equilibrium value of the CDW amplitude is given by $\Delta_{\rm eq}=1-(\phi_{\rm eq}-\phi_0/\theta)^2$. To first order in κ, linearization of the phase-slip equations gives

$$\sigma(\Omega')=\frac{1}{1+2\alpha\kappa(1-\Delta_{\rm eq})}\frac{i(\Omega'/\Omega_e)}{1+i(\Omega'/\Omega_c)}\ , \tag{2.13}$$

where $\Omega'=\Omega[1+2\alpha\kappa(1-\Delta_{\rm eq})]$ and $\Omega_c=\cos\phi_{\rm eq}+\alpha(3\Delta_{\rm eq}-2)$. Except for a change in the unit of time (of order $\alpha\kappa\ll 1$), the rigid-phase model yields an identical expression for $\sigma(\Omega)$ if $\beta=0$ and $F(\phi)=\sin\phi+\alpha(\phi-\phi_0)[1-(\phi-\phi_0/\theta)^2]$ in Eq. (2.12). Therefore the phase-slip equations have a pinned response that is overdamped.

When the CDW in the phase-slip equations is sliding, the elasticity term $\alpha\Delta(\phi-\phi_0)$ is essentially periodic in phase as long as the ac field is not large. In the limit that $\theta\gg 4\pi$ and $\alpha\gg(4\pi)^{-1}$, the pinning term $\sin\phi$ may be dropped from the phase-slip equations, which then reduce to

$$\dot\phi\cong e_{\rm dc}+e_{\rm ac}e^{i\Omega t}-\alpha\Delta(\phi-\phi_0)\ , \tag{2.6a'}$$

$$\Delta=[1-(\phi-\phi_0/\theta)^2]-\kappa\dot\Delta\ , \tag{2.6b'}$$

$$\phi_0\rightarrow\begin{cases}\phi_0 & \text{if } \phi-\phi_0<\theta\\ \phi_0+2\pi & \text{otherwise}\ .\end{cases} \tag{2.6c'}$$

Phase polarization in (2.6′) is bounded by $\theta-2\pi\le\phi-\phi_0\le\theta$, and therefore the elasticity term may be approximated by $\alpha\theta\Delta$ if terms of order $2\pi/\theta$ are neglected. Phase acceleration is then given by $\ddot\phi=i\Omega e_{\rm ac}e^{i\Omega t}-\alpha\theta\dot\Delta$, and substitution of this expression into Eq. (2.6a′) yields

$$\kappa\ddot\phi+\dot\phi=e_{\rm dc}+e'_{\rm ac}e^{i\Omega t}-F_0(\phi)\ , \tag{2.14}$$

where $F_0(\phi)=\alpha(\phi-\phi_0)[1-(\phi-\phi_0/\theta)^2]$ and $e'_{\rm ac}=e_{\rm ac}(1+i\Omega)$. Thus the sliding response of the phase-slip equations is determined by an effective inertial parameter equal to κ.

The constraints on α and θ that lead to Eq. (2.14) are not unreasonable, since values of $\alpha=0.2$ and $\theta=10\pi$ are consistent with experiments (see below). Because appropriate values of κ fall in the range 0.5–1.0, the phase-slip equations are dynamically overdamped when pinned, but underdamped when sliding. Therefore, the equations should exhibit a strong nonlinear response above threshold. For example, if the constraint on $e_{\rm ac}$ is ignored, then Eq. (2.14) predicts that the sliding phase-slip equations should exhibit period-doubling bifurcations, chaos, and broad inductive features in ac conductivity.[15,16] In the next section, we will show explicitly that these phenomena do indeed occur.

III. NUMERICAL ANALYSIS

A. Method

Analytical solutions to Eqs. (2.6) are difficult to obtain except in a few limiting cases. Therefore, we present the results of a numerical study of these equations. Usually we will be interested in the CDW response to combined ac and dc fields. When both ac and dc fields are present, it is convenient to rescale the unit of time in Eqs. (2.6). Writing the external field as $e=e_{\rm dc}+e_{\rm ac}\cos(\Omega t)$, we define a new time variable by $\tau=\Omega t$. The reduced phase-slip equations become

$$\omega_{\rm ext}\phi'=e_{\rm dc}+e_{\rm ac}\cos\tau-\sin\phi-\alpha\Delta(\phi-\phi_0)\ ,$$

$$\omega_{\rm ext}\Delta'=-\frac{1}{\kappa}\left\{\Delta-\left[1-\left[\frac{\phi-\phi_0}{\theta}\right]^2\right]\right\}\ , \tag{3.1}$$

$$\phi_0\rightarrow\begin{cases}\phi_0 & \text{if } \Delta>0\\ \phi_0\pm 2\pi & \text{otherwise}\ ,\end{cases}$$

where $\omega_{\rm ext}=\Omega/\Omega_0$. Primes indicate differentiation with respect to τ. If no ac field is present, $\omega_{\rm ext}$ may be set to 1.

Equations (3.1) were solved using a straightforward scheme. As long as a phase-slip did not occur, the equations were numerically integrated to find $\phi(\tau)$ and $\Delta(\tau)$. To account for phase slips, we halted integration whenever Δ became nonpositive. We then calculated the time that Δ crossed zero, allowed ϕ_0 to slip by $\pm 2\pi$, and then restarted integration from the zero-crossing time.

As Fourier transforms and Poincaré sections of Eqs. (3.1) were very sensitive to systematic errors generated by the computer code, we were careful to eliminate this effect from our solutions. In intervals where $\Delta>0$, Eqs. (3.1) were integrated using a double-precision (about 14 significant digits), fifth-order Runge-Kutta method. Variable step sizes were used in the integration, but absolute local errors were kept smaller than 4×10^{-8}. The zero-crossing time of Δ was estimated by fitting a seventh-order polynomial to $\Delta(\tau)$ and then using Newton's method to find the polymonial's zero. The corresponding phase ϕ was evaluated at the zero-crossing time by a similar fitting procedure. To avoid systematic errors and singularity problems, it was necessary to use 30 significant digits in evaluating the polynomial coefficients. After the pinned phase was slipped, integration was restarted with a small initial step size of $2\pi\times10^{-5}$ in order to minimize the effect of the code interruption.

To check the stability of our integration scheme, we added a small amount of Gaussian noise (standard deviation $\approx 2\pi\times10^{-5}$) to displacements in Δ and ϕ. The only observable effect was an increase in the background-noise level of our Fourier transforms; the general nature of the solutions (e.g., period 1, period 2, etc.) did not change. To check the accuracy of our solutions, we employed an alternate integration scheme: a variable-order (one through twelve) Adams method, with absolute local errors less than 8×10^{-10}, and twelfth-degree polynomials fits. We found no significant difference in results between the integration methods. These checks showed that our integration method was stable and that our systematic errors were negligible.

Apart from the issue of numerical accuracy, solutions to Eqs. (3.1) depend on the choice of initial conditions. In this study, we always used "sliding" conditions: the CDW was started from the state $\Delta=0$ and $\phi-\phi_0=\theta$ at $\tau=0$. We then allowed the system to relax over many periods of the CDW motion. Before computing any quantities of interest, we checked the stability of our solutions to a further increase in the number of relaxation periods. Experimentally, our initialization procedure corresponds to biasing a CDW far above threshold, and then reducing the bias to the desired electric field.

B. Parameter values

The phase-slip equations of (3.1) contain seven free parameters: four CDW parameters (α, κ, θ, and ϕ_0) and three external field parameters (e_{dc}, e_{ac}, and ω_{ext}). A complete study of CDW dynamics in this seven-dimensional parameter space would be tedious and prohibitively time consuming. In this paper, we will fix α, θ, ϕ_0, and ω, and vary only κ, e_{dc}, and e_{ac}. As discussed previously, an appropriate choice for α is 0.2. The value of the strongly pinned phase ϕ_0 is expected to have a trivial effect on CDW dynamics, so we will arbitrarily set $\phi_0=0$ (modulo 2π). The polarizability θ will be chosen so that hysteresis in our theoretical I-V curves is close to the amount of hysteresis observed experimentally. The relative magnitude of hysteresis is about equal to

$$(e_{t2}-e_{t1})/e_{t2}\cong 1-\frac{3\sqrt{3}}{2}\left[1-\frac{2\pi}{\theta}\right]\left[1-\left[1-\frac{2\pi}{\theta}\right]^2\right] .$$

We will use $\theta=5\times 2\pi$ since this value of θ gives $(e_{t2}-e_{t1})/e_{t2}\sim 0.25$, which is typical of experiment.[16] Finally, we will choose $\omega_{ext}=1$, which corresponds to an experimental frequency of about 100 MHz.

To estimate appropriate ranges for κ, e_{dc}, and e_{ac}, it is convenient to consider typical I-V curves obtained from Eqs. (3.1). Figure 2 shows traces of $\langle\phi'\rangle$ versus e_{dc} when $e_{ac}=0$ and κ varies from 0.5 to 1.0. As expected, the I-V curves exhibit both switching and hysteresis. Where the I-V curves are bistable, dashed and solid lines indicate, respectively, CDW current under monotonically increasing and decreasing bias. Lower and upper threshold fields are indicated in the top figure, as well as the magnitudes δ_1 and δ_2 of the lower and upper current switches.

As mentioned above, the parameter κ represents the relaxation time of a strongly pinned domain. Since a strongly pinned domain should respond at least as quickly as a weakly pinned domain, we expect $\kappa\lesssim 1$. Figure 2 shows that switching and hysteresis do not depend strongly on κ for $\kappa\gtrsim 0.5$. The main difference between the traces in Fig. 2 is the size δ_1 of the lower current switch and the position e_{t1} of the lower current threshold. As κ decreases, δ_1 decreases and e_{t1} slightly increases. In the limit that $\kappa\to 0$, δ_1 vanishes completely and there is only an $(e-e_{t1})^{1/2}$ cusp at the lower threshold. In experimental I-V curves, there is always a finite current jump at the lower threshold, so we will consider only nonvanishing values of κ in the range 0.2–1.0.

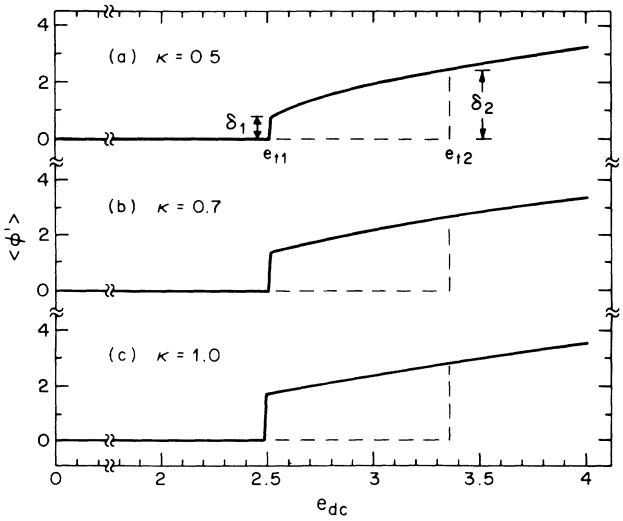

FIG. 2. I-V curves $\langle\phi'\rangle$ vs e_{dc} obtained from the reduced phase-slip equations (3.1). The applied ac field is zero and the amplitude relaxation rate assumes three representative values: (a) $\kappa=0.5$, (b) $\kappa=0.7$, and (c) $\kappa=1.0$. (In this figure and the figures which follow, the other phase-slip parameters are fixed at $\alpha=0.2$, $\theta=10\pi$, $\phi_0=0$, and $\omega_{ext}=1.0$.)

Under the application of an ac electric field, the I-V curves of Fig. 2 display a series of plateaus or "Shapiro steps."[22] On the nth Shapiro step, CDW velocity is mode locked to the nth harmonic of the external frequency: $\langle\dot\phi\rangle=n\omega_{ext}$. We will arbitrarily limit e_{dc} to the range that corresponds to the fourth Shapiro step. Since the width of a Shapiro step depends on the amplitude of the applied ac field, we choose (again arbitrarily) e_{ac} to be in the range $e_{t2}\lesssim e_{ac}\lesssim 2e_{t2}$. With this choice, e_{dc} lies in the range 4.0–5.5. Figure 3 summarizes the parameter ranges used in this study.

C. Chaos and period doubling

The response of the phase-slip equations to combined ac and dc fields is qualitatively different depending on whether the ac field is large ($e_{ac}\gtrsim 1$) or small ($e_{ac}\ll 1$). With small ac fields, the CDW phase velocity is not entrained by the external frequency. Two independent frequencies characterize the phase velocity, which may be written as a double Fourier series:

$$\dot\phi(t)=\omega_N\sum_{l=0}^{\infty}A_l\cos(l\omega_N t+\chi_l)+\sum_{m=0}^{\infty}B_m\cos(m\omega_{ext}t+\chi_m) . \quad (3.2)$$

Here ω_N is the so-called washboard frequency and is equal to the time-averaged phase velocity $\langle\phi'\rangle$. When e_{ac} is small, ω_N is essentially determined only by the dc electric field. Except at special values of e_{dc}, the external ac frequency is incommensurable with the washboard frequency, so the CDW phase velocity is a quasiperiodic function of time.

With large ac fields, the CDW phase velocity mode locks to the external frequency over wide ranges of dc bias.[23] When the CDW is mode locked, the CDW washboard frequency is a rational fraction of the external frequency,

$$\omega_N\equiv\langle\phi'\rangle=(p/q)\omega_{ext} ,$$

and the CDW phase velocity may be written as

$$\dot\phi(t)=\omega_N\sum_{n=0}^{\infty}C_n\cos(n\omega_N t/P+\chi_n) .$$

Here, P is an integer index characterizing the fundamental periodicity of CDW motion with respect to the external frequency. When $P=1$, CDW motion is described as period 1; when $P=2$, as period 2; and so on.

In this section, we examine the effect of large ac fields on the phase-slip equations of (3.1). We begin by fixing the amplitude relaxation time to a moderate value: $\kappa=0.5$. (We investigate the effect of κ later in this section.) We then vary the applied ac and dc bias over the vertical parameter plane shown in Fig. 3. We characterize solutions to (3.1) by their mode-locking index $p/q=\langle\phi'\rangle/\omega_{\rm ext}$ and their periodicity index P. Figure 4 summarizes the type of solutions found in the $e_{\rm dc}$-$e_{\rm ac}$ plane. Typically, solutions are periodic and mode locked to harmonic ($p/q=$integer) Shapiro steps. We use the symbol (n,P) to represent these solutions, where the integer n is $\langle\phi'\rangle/\omega_{\rm ext}$. Other solutions in this region are chaotic but still harmonically mode locked, and we represent these solutions by (n,C). The remaining solutions in the parameter plane correspond to quasiperiodic motion or subharmonic ($p/q\neq$integer) Shapiro steps. For simplicity, we denote these solutions by (Q/S) and represent them by blank areas in Fig. 4.

In a typical experiment on CDW's, the amplitude of the ac field is fixed and the dc bias is swept through a range of values. To facilitate comparison with experiment, we will discuss Fig. 4 in terms of dc sweeps. For instance, the horizontal line in Fig. 4 corresponds to a dc sweep in which the ac amplitude is fixed at 4.5. (This line also corresponds to the intersection of the horizontal and vertical parameter planes in Fig. 3.) As $e_{\rm dc}$ increases along this line, solutions move from the third Shapiro step, through the fourth Shapiro step and an unlocked region, and finally onto the fifth Shapiro step:

$$(3,1)\rightarrow(4,P\geq 1)\rightarrow(Q/S)\rightarrow(5,1)\ .$$

Figure 5 shows the details of this dc sweep. The dashed line in the figure represents the entrainment ratio $\langle\phi'\rangle/\omega_{\rm ext}$. Over most of the figure, solutions are mode locked to a harmonic step. For example, the third Shapiro step extends from $e_{\rm dc}\cong 4.0$ to 4.3, the fourth Shapiro step from 4.3 to 5.3, and the fifth step from 5.4 to 5.5. Harmonic mode locking breaks down only between $e_{\rm dc}\cong 5.3$ and 5.4.

The solid line in Fig. 5 represents the periodicity index P. (We adopt a convention of assigning $P=0$ to solutions where periodic behavior is not observed, including both chaotic and quasiperiodic solutions.) Even though solutions are usually mode locked in Fig. 5, the periodicities of the solutions are often not 1. In fact, the most important feature of Fig. 5 is the region of locked but aperiodic solutions that occurs on the fourth Shapiro step. Between $e_{\rm dc}\cong 4.3$ and 4.53, solutions follow a period-doubling cascade to chaos:

$$(4,1)\rightarrow(4,2)\rightarrow(4,4)\rightarrow\cdots\rightarrow(4,C)\ .$$

Between $e_{\rm dc}\cong 4.6$ and 5.3, solutions return to simple periodicity via a period-halving cascade:

$$(4,C)\rightarrow\cdots\rightarrow(4,4)\rightarrow(4,2)\rightarrow(4,1)\ .$$

Although the figure only resolves periodicities of up to $P=8$, solutions with periodicities of up to $P=32$ were confirmed by Fourier transforms. Figures 6(a)–6(c) show a few of these transforms, for $P=1$, 2, and 32 at

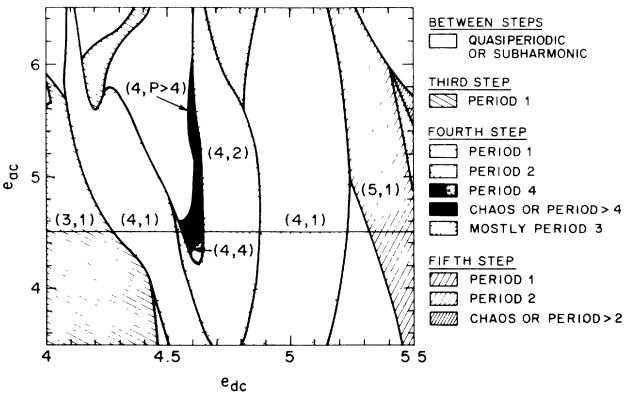

FIG. 4. A schematic picture of the solutions that are found in the $e_{\rm dc}$-$e_{\rm ac}$ plane of Fig. 3. Harmonically mode-locked solutions are characterized by an index pair (n,P) which represents their entrainment n and periodicity P. (Boundaries between different regions are only approximate.) The horizontal line represents the intersection of parameter planes in Fig. 3.

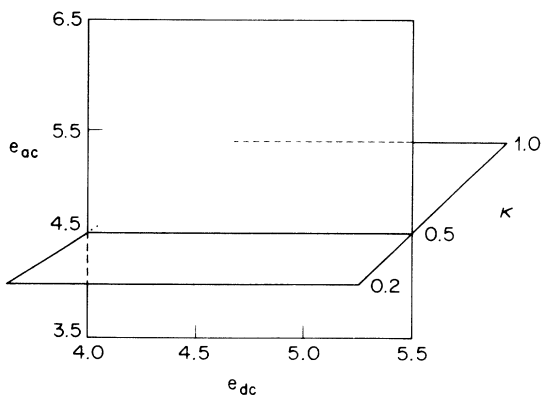

FIG. 3. The parameter planes that are studied in this paper.

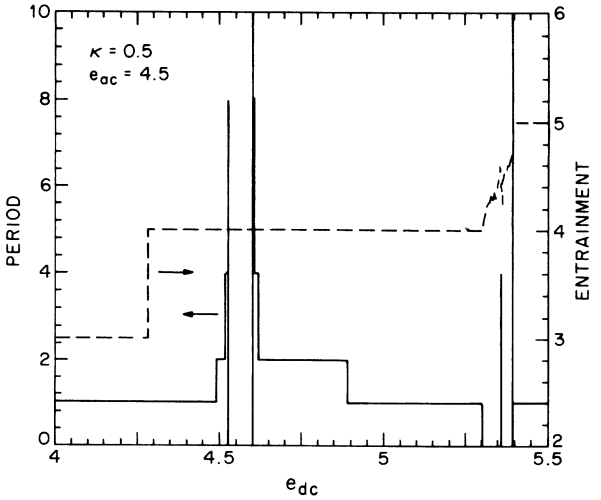

FIG. 5. A dc sweep along the intersection of parameter planes in Fig. 3. The dashed and solid lines indicate, respectively, the entrainment and periodicity of solutions found in this range of dc bias.

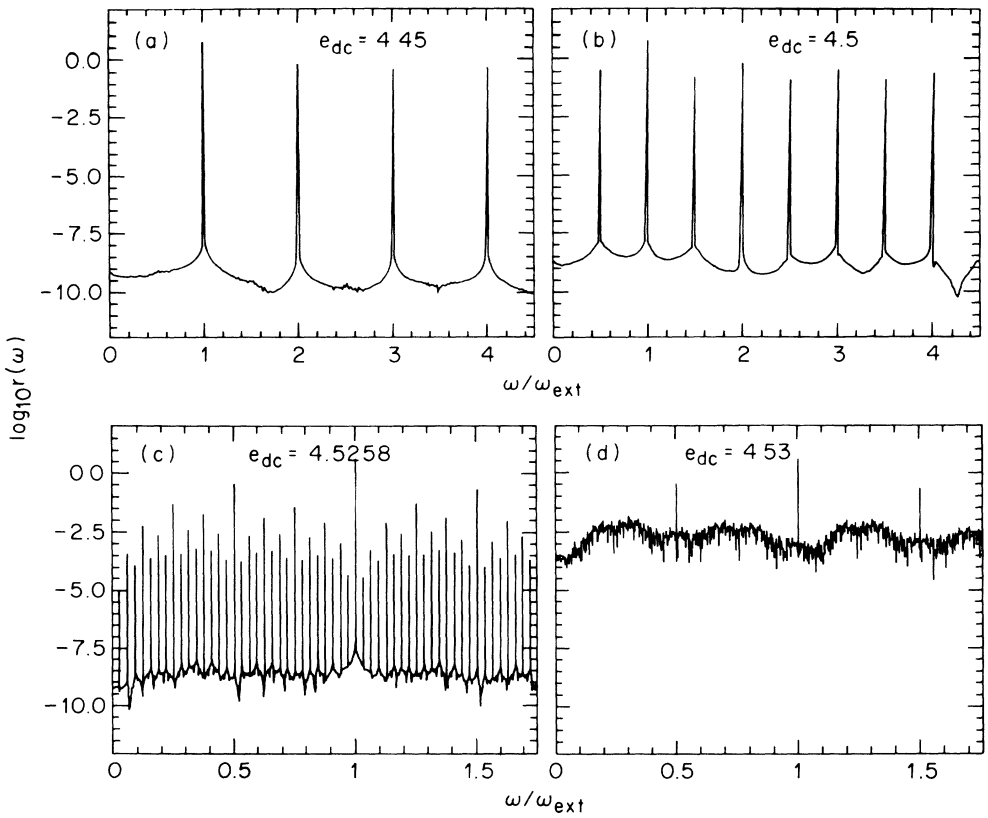

FIG. 6. Fourier transforms for selected solutions from Fig. 5. The vertical scale represents the amplitude of the transformed phase velocity $r(\omega)=|\tilde{\dot{\phi}}|$. Although all of the selected solutions are mode locked to the fourth Shapiro step, the solutions are part of a period-doubling cascade to chaos: (a) period 1 ($e_{dc}=4.45$), (b) period 2 ($e_{dc}=4.5$), (c) period 32 ($e_{dc}=4.5258$), and (d) chaos ($e_{dc}=4.53$). The horizontal scale has been expanded in the lower figures in order to show the details of these transforms.

$e_{dc}=4.45$, 4.5, and 4.5258, respectively. Note that the noise level in these transforms is smaller than $\sim 10^{-8}$. In contrast, solutions are chaotic for e_{dc} between 4.53 and 4.6. Figure 6(d) shows the Fourier transform of a typical chaotic solution, at $e_{dc}=4.53$. The noise level is roughly 10^{-2}, 6 orders of magnitude larger than the noise level of periodic solutions. Because of this large increase in noise, chaotic solutions are clearly distinguished from periodic or quasiperiodic solutions.

Having considered a particular dc sweep in detail, we now return to Fig. 4 to discuss the general behavior of solutions at other values of e_{ac}. As the ac amplitude decreases below 4.5, Fig. 4 shows that the chaotic region shrinks on the fourth Shapiro step. Below $e_{ac}\cong 4.2$, only period-1 and period-2 solutions exist on the fourth-step. Also, as e_{ac} decreases, the unlocked regions between steps become larger. Below $e_{ac}\simeq 4.0$, for example, an unlocked region develops between the third and fourth Shapiro steps. As would be expected, Fig. 4 suggests that only period-1 and quasiperiodic solutions exist for small ($\lesssim 3$) values of e_{ac}.

As e_{ac} increases above 4.5, chaotic solutions remain present until e_{ac} exceeds about 6. However, period doubling and chaotic solutions begin to be unstable against mode dephasing above $e_{ac}\cong 4.6$. Thus in the range $4.6\lesssim e_{ac}\lesssim 6.0$, the fourth Shapiro step is split by a region of quasiperiodic and subharmonic solutions. For instance, a typical dc sweep at $e_{ac}=5.0$ produces a sequence like

$$(3,1)\rightarrow(4,1)\rightarrow(Q/S)\rightarrow(4,C)\rightarrow\cdots\rightarrow(4,1)\rightarrow(5,1)\ .$$

Due to the system's strong tendency to mode lock, subharmonic Shapiro steps occupy much of the region marked (Q/S) in the sequence. In fact, for $e_{ac}\gtrsim 5.6$, the system begins to relock to the $n=3$ Shapiro step when it is not locked to the $n=4$ step.

Two new types of solutions appear at large values of e_{ac}. The first type of solution corresponds to $P>1$ solutions on the $n=5$ Shapiro step. For example, when $e_{ac}\cong 5.6$, a sweep of dc bias encounters two regimes of chaotic solutions:

$$(3,1)\rightarrow(4,1)\rightarrow(Q/S)\rightarrow(4,C)\rightarrow\cdots\rightarrow(4,1)\rightarrow(5,1)\rightarrow(5,2)\rightarrow\cdots\rightarrow(5,C)\ .$$

The second type of solution corresponds to periodicities of the form $P=p\times 2^n$, where p is a prime number. Although p can be as large as 19, the dominant periodicity of this form is $P=3$. The disappearance of chaotic solutions at $e_{ac}\cong 6$ coincides with the proliferation of $P=3$ solutions beyond this point.

On a heuristic level, the disappearance of chaotic solutions at either large or small values of e_{ac} is reasonable. In Eqs. (3.1), three ingredients are apparently required

for chaos. The most basic ingredient is a nonzero value of κ, as will be discussed shortly. The next ingredient is that the system is close to the center of a Shapiro step. The last ingredient is that e_{ac} and e_{dc} are of comparable magnitude. This last ingredient is required because chaotic motion in some sense represents a frustrated response of the system, when neither e_{ac} nor e_{dc} dominates the CDW equation of motion. When the system is near the center of a Shapiro step, this frustration is not easily relieved by changing the system's degree of mode locking. Thus chaotic solutions appear in Fig. 4 when e_{ac} and e_{dc} are roughly comparable and near the center of a Shapiro step, at $e_{ac} \cong e_{dc} \cong 4.5$ and 5.5.

We next discuss the sensitivity of chaotic and $P > 1$ solutions to changes in κ. In the limit that $\kappa \to 0$, the CDW amplitude becomes a deterministic function of the CDW phase polarization:

$$\Delta \to 1 - \left[\frac{\phi - \phi_0}{\theta} \right]^2 .$$

In this limit, the phase space of Eqs. (3.1) becomes two dimensional. Therefore, the equations are unable to support chaotic solutions. This conclusion agrees with the observed absence of chaotic solutions in the overdamped rigid-phase model.

The presence or absence of $P > 1$ solutions is not obvious when κ is small but nonzero. We have therefore investigated the nature of solutions found in the e_{dc}-κ plane shown in Fig. 3, where $0.2 \le \kappa \le 1.0$, $4.0 \le e_{dc} \le 5.5$, and $e_{ac} = 4.5$. Figure 7 summarizes the solutions found in this plane.

The structure of solutions in Fig. 7 is much simpler than the structure in Fig. 3. A series of entrainment "tongues" is clearly evident. The $n = 3$, 4, and 5 Shapiro steps form three tapered, vertical strips. As κ decreases, these "tongues" become narrow and the quasiperiodic regions between them become wider. Conversely, as κ increases, the tongues become wider and subtongues develop within them. The first subtongue to form is the period-2 strip within the four Shapiro step; the next subtongue is a period-4 strip within the period-2 tongue; and so on. When $\kappa = 0.5$, the dc sweep of Fig. 5 shows that a chaotic subtongue is fully developed within the fourth Shapiro step. Because the tongue structure is stable above $\kappa \cong 0.4$, Fig. 5 suggests that the phase-slip equations of (3.1) are relatively insensitive to κ for $\kappa \gtrsim 0.4$.

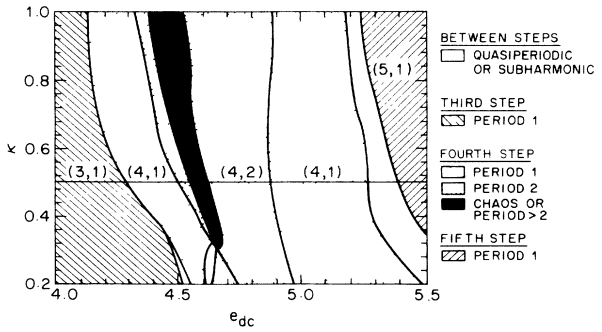

FIG. 7. Solutions in the e_{dc}-κ plane of Fig. 3. The horizontal line marks the intersection with the e_{dc}-e_{ac} plane of Fig. 4.

D. ac conductivity

In this section, we examine the response of the phase-slip equations to small ac fields. The effect of small ac fields is best measured by ac conductivity, which we now define as

$$\sigma(\omega_{ext}) = \tilde{\dot{\phi}}(\omega_{ext})/e_{ac} . \tag{3.3}$$

When the CDW is sliding, a complication to computing $\sigma(\omega_{ext})$ is that a dc field causes the CDW phase velocity to oscillate at the washboard frequency, even in the absence of an ac field. This phenomenon is known as "narrow-band noise."[6,24] In Eq. (3.2), for example, the CDW phase velocity has a Fourier component $\omega_N A_1$ at the washboard frequency ω_N. The amplitude of this component is about 1. Hence, if a small ac field is applied with a frequency that matches the CDW washboard frequency, our definition of $\sigma(\omega_{ext})$ diverges in the limit that $e_{ac} \to 0$:

$$|\sigma(\omega_{ext} = \omega_N)| \sim \frac{1}{e_{ac}} .$$

Our definition of $\sigma(\omega_{ext})$ similarly diverges at the second, third, and higher harmonics of ω_N. Although we could redefine $\sigma(\omega_{ext})$ to eliminate these divergences, the definition in (3.3) corresponds to how ac conductivity is actually measured in experiment. Therefore we will continue to use (3.3) to define $\sigma(\omega_{ext})$, even in the sliding regime of the phase-slip equations.

The sliding ac conductivity of the phase-slip equations is displayed in Fig. 8 for two values of the ac test signal. For the calculations in this figure, the amplitude relaxation rate was fixed at $\kappa = 0.5$ and the other phase-slip parameters remained $\alpha = 0.2$ and $\theta = 10\pi$. The dc bias was $e_{dc} = 2.6$, which is about 104% of the lower threshold field e_{t1}.

Figure 8(a) shows $\sigma(\omega_{ext})$ when the ac test signal is 1% of the lower threshold field. Sharp resonance are present in Reσ and Imσ at the washboard frequency and its harmonics. Near the washboard frequency, $\omega_N = 1.13$, the main effect of the test signal is to fix the phase of the narrow-band noise relative to the test frequency. Thus the magnitude of $\sigma(\omega_{ext})$ is constant near ω_N and roughly equal to $1/e_{dc}$. At frequencies below ω_N, the in-phase component of $\sigma(\omega_{ext})$ is equal to the slope $d\langle\dot{\phi}\rangle/de_{dc}$ of the I-V curve, while the out-of-phase component of $\sigma(\omega_{ext})$ is zero. At high frequencies, Imσ goes to zero when ω_{ext} is not close to a harmonic of the washboard frequency. Although not apparent in Fig. 8(a), Reσ goes to 1 at high frequencies.

Figure 8(b) shows $\sigma(\omega_{ext})$ when the ac test signal has increased to 5% of e_{t1}. New subharmonic resonances are present at $\frac{2}{3}\omega_N$ and $\frac{3}{2}\omega_N$, and the harmonic resonances at $2\omega_N$, $3\omega_N$, and $4\omega_N$ are now much larger. More importantly, the fundamental resonance at $\omega_{ext} = \omega_N$ is no longer sharp. The real and imaginary components of $\sigma(\omega_{ext})$ display broad regions in which conductivity de-

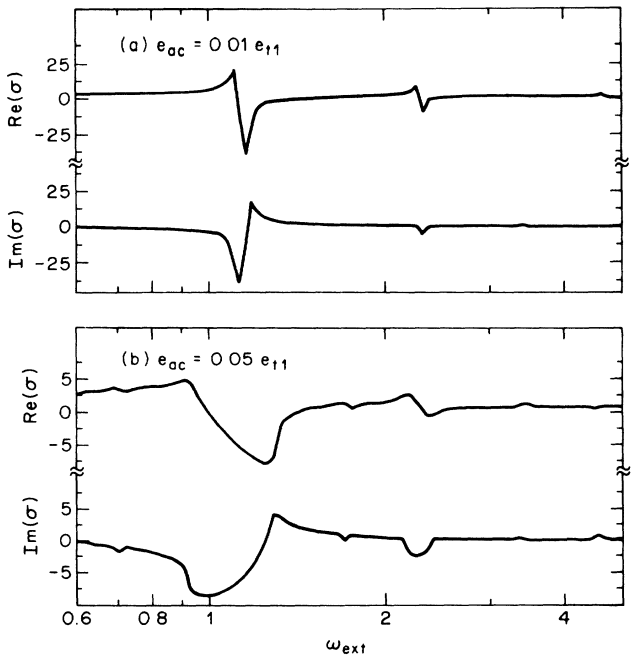

FIG. 8. Sliding ac conductivity of the reduced phase-slip equations. The conductivity is sensitive to mode locking, as shown by the effect of an increasing ac test signal: (a) $e_{dc}=0.01e_{t1}$ and (b) $e_{dc}=0.05e_{t1}$.

creases with increasing frequency. Furthermore, Imσ is negative over a wide frequency range, from $\omega_{ext}=0.6$ to $\omega_{ext}=1.2$. An inductive response (i.e., Im$\sigma<0$) over such a wide frequency range is unusual in an overdamped model of CDW dynamics. Inductive behavior is observed in overdamped classical models,[6,7] as well as the quantum tunneling model,[8] but only over narrow frequency ranges. The widths of inductive dips in these modes are typically 10% or less of ω_N, regardless of the test signal magnitude. In Fig. 8(b), the width of the inductive region is over 50% of ω_N.

IV. COMPARISON OF THEORY AND EXPERIMENT

In this section, we will examine the agreement between predictions of the phase-slip equations and experimental results on switching crystals. We will limit our comparison to experiments on $NbSe_3$, since switching has been extensively characterized in this material.

The best quantitative agreement between theory and experiment is obtained for singly applied ac or dc fields. For example, the I-V characteristic of Fig. 2(a) matches the $NbSe_3$ I-V curve in Fig. 1 of Ref. 16 quite closely. In both I-V curves, the differential conductance dI/dV is constant past the upper threshold field, the hysteresis loop extends over a bias range which is about 25% as large as the threshold field, and the ratio of upper to lower current switches is about 4:1. This agreement is trivial, of course, since it is built into the phase-slip equations. In both the phase-slip model and real crystals, switching is (arguably) caused by an effective collapse of the CDW pinning potential. This effective collapse produces a constant dI/dV past threshold. And the phase-slip parameters α, θ, and κ allow the I-V characteristic of the phase-slip equations to be adjusted arbitrarily. Since the phase-slip equations can therefore fit any single-switch I-V characteristic of $NbSe_3$, the shape of dc I-V curves is not a critical test of the phase-slip model. (Some I-V characteristics of $NbSe_3$ display more than one switch,[14] a point to which we will return shortly.)

A nontrivial point of agreement, however, is the relative size of switching versus nonswitching threshold fields. A comparison of threshold fields is difficult to make experimentally because of large sample-to-sample variations, even among nonswitching crystals. In $NbSe_3$, comparison can be made indirectly by studying the temperature dependences of threshold fields.[14] In the lower CDW state of nominally pure crystals, switching is never observed at 48 K, but is usually observed (if it is observed at all) when the crystal temperature is lowered to 30 K. In nonswitching crystals, threshold fields typically increase by a factor of 3 as the temperature is lowered from 48 to 30 K. In contrast, threshold fields in switching crystals typically increase by a factor of 10 over this temperature range. The onset of switching is therefore experimentally associated with a threefold increase in threshold field. (Some experiments on cleaved crystals also point to a ratio of 3:1 between switching and nonswitching thresholds.[14])

In the phase-slip model, switching is caused by the coupling of a weakly pinned domain to a strongly pinned domain. When this coupling is absent, the nonswitching threshold field is 1. But if this coupling is present, and if the phase-slip parameters are chosen to reproduce experimental I-V characteristics, then the switching threshold field is about 3. Thus threshold fields in the phase-slip model are 3 times larger for switching than for nonswitching CDW's. This agreement with experiment is significant, because other models require threshold fields that are up to 1000 times larger for switching than for nonswitching CDW's.[14]

The pinned ac conductivity of the phase-slip model also agrees quite closely with experiment. In $NbSe_3$, the pinned ac conductivity of either switching or nonswitching crystals is described reasonably well by the frequency dependence of Eq. (2.13). Furthermore, the crossover frequencies in switching and nonswitching crystals are equal to within the uncertainty of sample-to-sample fluctuations. In the phase-slip model, Eq. (2.13) applies to both switching and nonswitching CDW's, and crossover frequencies are shifted by only $\sim$20% because of switching.

For jointly applied ac and dc fields, nonlinear instabilities are a distinguishing feature of switching in both theory and experiment. In $NbSe_3$ crystals, period doubling and chaos are observed only in switching crystals.[16] In the phase-slip model, period doubling and chaos occur only when $\theta>\theta_H$ and $\kappa>0$, i.e., only when the phase-slip equations predict switching. Theory and experiment also agree on other qualitative aspects of chaotic dynamics. For instance, nonlinear instabilities are associated with period-doubling routes to chaos, rather than quasiperiodic routes, chaotic states remain mode locked to Shapiro

steps, and period-doubling routes to chaos occur on each Shapiro step when the dc bias is comparable to the ac field. In addition, the external field parameters required for chaotic motion are comparable in theory and experiment. In $NbSe_3$, period-doubling bifurcations or chaos have been observed at ac frequencies between 0.5 and 50 MHz, and for ac fields between 50 and 100% of the threshold field.[16] In this paper, chaos occurs at an ac frequency comparable to 100 MHz and for ac fields between 100 and 200% of the threshold field.

Both switching $NbSe_3$ crystals and the phase-slip equations exhibit a strong tendency to mode lock to external ac signals. At temperatures where switching is prominently developed in $NbSe_3$, Shapiro steps are much broader (as a function of dc bias) than they are at higher temperatures.[16] In the switching regime, the regions of dc bias between harmonic Shapiro steps are so narrow that quasiperiodic or subharmonically locked CDW motion cannot be resolved. Furthermore, strong mode locking in $NbSe_3$ is closely correlated with chaotic dynamics. As the temperature of a $NbSe_3$ crystal is raised above the switching regime, Shapiro steps become narrower and nonlinear instabilities gradually disappear. Similar mode-locking characteristics are displayed by the phase-slip equations. In the parameter regime where switching occurs ($\theta > \theta_H$), Shapiro steps are much broader than in the overdamped Grüner-Zawadowski-Chaikin model, which is the nonswitching ($\theta \rightarrow 0$) limit of the phase-slip equations. In the switching regime of the phase-slip equations, no unlocked regions are observed between some Shapiro steps; for example, between the third and fourth steps in Fig. 5. And finally, strong mode locking appears to be a prerequisite for nonlinear instabilities in the phase-slip equations, as was discussed in Sec. III.

The last point of agreement between theory and experiment is the inductive behavior observed in sliding ac conductivity measurements. Two characteristics distinguish the sliding ac conductivity of switching crystals from that of nonswitching crystals.[15] For frequencies below the washboard frequency, $\mathrm{Im}\sigma(\omega)$ is negative, and both $\mathrm{Im}\sigma(\omega)$ and $\mathrm{Re}\sigma(\omega)$ decrease with increasing frequency. The same behavior is displayed by the phase-slip equations in Fig. 8(b). In addition, the qualitative difference in $\sigma(\omega)$ between Figs. 8(a) and 8(b) suggests that inductive behavior is due to a nonlinear interaction of the phase-slip equations with the applied ac test signal. Indeed, additional calculations have shown that broad inductive clips in $\sigma(\omega)$ are caused by mode locking between the external frequency and the CDW washboard frequency.[25] Preliminary experiments on $NbSe_3$ suggest that inductive behavior in switching crystals is also dependent on the ac test signal.[26]

In some important aspects, however, the behavior of the reduced phase-slip equations differs significantly from that of $NbSe_3$ switching crystals. There are several discrepancies in sliding ac conductivity, for example. In experiment,[15] unlike the reduced equations, the in-phase component of $\sigma(\omega)$ is never negative, the low-frequency limit of $\mathrm{Re}\sigma(\omega)$ is less than the high-frequency limit, the out-of-phase component of $\sigma(\omega)$ does not go to zero at high frequencies, and the inductive dip in $\mathrm{Im}\sigma(\omega)$ occurs over a frequency range much wider than $0.5\omega_N$. There is also qualitative disagreement over the features of nonlinear instabilities. Deterministic noise in the phase-slip model is much larger than the chaos observed experimentally.[16] *Complete* period-doubling cascades have not been observed in $NbSe_3$, and period-halving cascades, whether complete or incomplete, are totally absent.[16] Small regions of period-3 or period-5 response may be present in some crystals, but these regions occupy a much smaller amount of parameter space than shown in Fig. 4.[16] Even in dc response, the reduced phase-slip equations differ from experiment, because some $NbSe_3$ crystals display multiple, rather than just single, switches in their I-V characteristics.[14]

Many of these discrepancies, however, can be traced to the neglect of internal CDW degrees of freedom. The reduced phase-slip equations treat the weakly pinned regions of a CDW as rigid. Experiments on nonswitching CDW's show that this is a crude approximation. A better approximation is to treat weakly pinned regions as internally deformable. Inclusion of internal CDW modes has several important effects on CDW dynamics.[27] First, narrow-band noise is suppressed. The relative amplitude of narrow-band noise decreases as $1/\sqrt{N}$ where N is the number of internal CDW modes. Second, the dc conductivity near threshold changes from an $(E-E_T)^{1/2}$ to an $(E-E_T)^{\nu}$ behavior, where $\nu > 1$. As a result, the differential conductivity dI/dV remains finite and less than the high-field, high-frequency limit. Third, the high-frequency ac conductivity becomes dominated by internal CDW modes. Consequently, the sliding ac conductivity approaches the pinned ac conductivity at frequencies larger than the washboard frequency.

The complete phase-slip equations, Eqs. (2.5), should give much closer agreement with experiment than the reduced equations. In the complete equations, the weakly pinned regions of a CDW are deformable. The sliding ac conductivity of the complete equations will be improved, therefore, over that of the reduced equations. The out-of-phase component of $\sigma(\omega)$ will be nonzero at high frequencies, since it will approach its pinned value. The in-phase component of $\sigma(\omega)$ will be smaller at low frequencies than high frequencies, since dI/dV is reduced by internal CDW modes. Finally, $\mathrm{Re}\sigma(\omega)$ will remain positive at all frequencies, at least for reasonable values of the ac test signal. Negative values of $\mathrm{Re}\sigma(\omega)$ occur because the narrow-band noise signal is larger than the in-phase CDW response. In real experiments, narrow-band noise is typically 100 or 1000 times smaller than $V_{\mathrm{ac}}(dI/dV)$, where V_{ac} is the amplitude of the applied ac field. [The current $V_{\mathrm{ac}}(dI/dV)$ represents a lower bound on the in-phase CDW response.] If narrow-band noise is comparably small in the complete phase-slip equations, $\mathrm{Re}\sigma(\omega)$ will not be negative.

The complete phase-slip equations should also yield more realistic levels of deterministic noise. Bifurcations and chaos in the phase-slip model are due to the dynamical instability of phase elasticity. In the complete phase-slip equations, however, the majority of phase-phase coupling terms will not be driven into the regime of unstable

elasticity. By a simple counting argument, the relative amplitude of deterministic noise should decrease as the fraction of unstable coupling terms decreases.

An interesting question is whether, in the complete phase-slip equations, period-doubling cascades will be truncated, period-halving cascades will be eliminated, and period-3 responses will be suppressed. The introduction of random noise into deterministic dynamical systems is known to produce these effects. And real CDW systems are known to exhibit broadband noise that is induced by CDW transport.[28] If the introduction of internal CDW modes were known to cause broadband noise, then one might speculate that this broadband noise could indeed truncate bifurcation cascades. Unfortunately, internal CDW modes alone do not lead to broadband noise.[29] However, deformable CDW models are only marginally stable against the development of broadband noise.[29] The presence of some highly nonlinear phase-phase coupling terms could include broadband noise, which would in turn truncate bifurcation cascades. If this scenario is correct, then the complete phase-slip equations would not only provide more realistic levels of chaos, but they would also provide an explanation of the origin of broadband noise.

As a final observation, the complete phase-slip equations provide an obvious mechanism for multiple switching by a CDW.[14] Instability of the phase-mode elasticity can occur independently at each strong-pinning site within a crystal, and hence each strong-pinning site can produce a switch. In real crystals, apparently single switches in an I-V characteristic are often the result of an avalanche of switches at multiple strong-pinning sites. A distribution of strong-pinning centers, along with an associated distribution of phase-slip parameters, could also explain the wide frequency range of the inductive dip in $\mathrm{Im}\sigma(\omega)$.

wide frequency range of the inductive dip in $\mathrm{Im}\sigma(\omega)$.

In summary, we have shown that the reduced phase-slip equations of (3.1) display switching, hysteresis, period doubling, chaos, and an inductive ac conductivity. These phenomena are observed experimentally in switching $NbSe_3$ crystals, and in this section we have discussed the qualitative agreement between experiment and the phase-slip hypothesis. By way of conclusion, the overall consistency of the phase-slip model should be emphasized. Switching crystals are the only class of CDW conductor in which dc electric fields have been demonstrated to produce CDW current discontinuties. Current discontinuities, in turn, require fluctuations of the CDW amplitude. Significantly, the dynamics of switching CDW's have not been self-consistently explained on the basis of CDW phase dynamics alone. On the other hand, amplitude fluctuations are a starting point of the phase-slip equations, and lead directly to the phenomena which characterize transport in real switching crystals. Thus, the phase-slip equations provide a self-consistent model of switching which is also in good qualitative agreement with experiment.

ACKNOWLEDGMENTS

We thank D. Browne, P. Bryant, S. Coppersmith, L. M. Falicov, M. H. Hundley, P. B. Littlewood, and M. S. Sherwin for valuable discussions and useful comments. This work was supported by National Science Foundation Grant No. DMR-86-13180. We acknowledge the San Diego Supercomputer Center at GA Technologies, Inc. and the National Center for Supercomputing Applications at the University of Illinois at Urbana-Champaign for access to their facilities.

[1]For a recent review of the subject, see G. Grüner and A. Zettl, Phys. Rep. **119**, 117 (1985).

[2]P. A. Lee, T. M. Rice, and P. W. Anderson, Solid State Commun. **14**, 703 (1974).

[3]H. Fukuyama, J. Phys. Soc. Jpn. **41**, 513 (1976).

[4]H. Fukuyama and P.A. Lee, Phys. Rev. B **17**, 535 (1978).

[5]Hamiltonians similar to Eq. (2.1) were written down previously by W. L. McMillan, Phys. Rev. B **12**, 1187 (1975); P. A. Lee and T. M. Rice, *ibid.* **19**, 3970 (1979). An equation of motion similar to Eq. (2.3) was first written down by W. L. McMillan, Phys. Rev. B **12**, 1197 (1975).

[6]G. Grüner, A. Zawadowski, and P. M. Chaikin, Phys. Rev. Lett. **46**, 511 (1981).

[7]Leigh Sneddon, M. C. Cross, and Daniel S. Fisher, Phys. Rev. Lett. **49**, 292 (1982).

[8]J. Bardeen, Phys. Rev. Lett. **42**, 1498 (1979); **55**, 1010 (1985).

[9]N. P. Ong, G. Varma, and K. Maki, Phys. Rev. Lett. **52**, 663 (1984); N. P. Ong and K. Maki, Phys. Rev. B **32**, 6582 (1985).

[10]L. P. Gor'kov, Pis'ma Zh. Eksp. Teor. Fiz. **38**, 76 (1983) [JETP Lett. **38**, 87 (1983)]; I. Batistic, A. Bjelis, and L. P. Gor'kov, J. Phys. (Paris) **45**, 1049 (1984).

[11]R. P. Hall, M. F. Hundley, and A. Zettl, Phys. Rev. Lett. **56**, 2399 (1986).

[12]M. F. Hundley and A. Zettl, Phys. Rev. B **33**, 2883 (1986).

[13]A. Zettl and G. Grüner, Phys. Rev. B **26**, 2298 (1982).

[14]R. P. Hall, M. F. Hundley, and A. Zettl, this issue, Phys. Rev. B **38**, 13 002 (1988).

[15]R. P. Hall and A. Zettl, Solid State Commun. **50**, 813 (1984); R. P. Hall and A. Zettl, this issue, Phys. Rev. B **38**, 13 019 (1988).

[16]R. P. Hall, M. S. Sherwin, and A. Zettl, Phys. Rev. B **29**, 7076 (1984); M. S. Sherwin, R. P. Hall, and A. Zettl, preceding paper, Phys. Rev. B **38**, 13 028 (1988).

[17]R. P. Hall, M. F. Hundley, and A. Zettl, Physica **143B**, 152 (1986).

[18]S. Sridhar, D. Reagor, and G. Grüner, Phys. Rev. Lett. **55**, 307 (1985).

[19]W. J. Skocpol, M. R. Beasley, and M. Tinkham, J. Low Temp. Phys. **16**, 145 (1974).

[20]P. W. Anderson, Rev. Mod. Phys. **38**, 298 (1966).

[21]A. Zettl and G. Grüner, Phys. Rev. B **25**, 2081 (1982).

[22]S. Shapiro, Phys. Rev. Lett. **11**, 80 (1963); A. Zettl and G. Grüner, Solid State Commun. **46**, 501 (1983).

[23]For a general discussion of entrainment, period doubling, and chaos, see J. Guckenheimer and P. Holms, *Nonlinear Oscillations, Dynamical Systems, and Bifurcations of Vector Fields* (Springer-Verlag, New York, 1983).

[24]R. M. Fleming and C. C. Grimes, Phys. Rev. Lett. **42**, 1423 (1979).

[25]M. Inui and S. Doniach (unpublished).

[26]R. P. Hall and A. Zettl (unpublished).
[27]D. S. Fisher, Phys. Rev. B **31**, 1396 (1985); Leigh Sneddon, *ibid.* **29**, 725 (1984).
[28]P. Monceau, J. Richard, and M. Renard, Phys. Rev. B **25**, 931 (1982).
[29]P. Littlewood, Phys. Rev. B **33**, 6694 (1986), and private communcation.

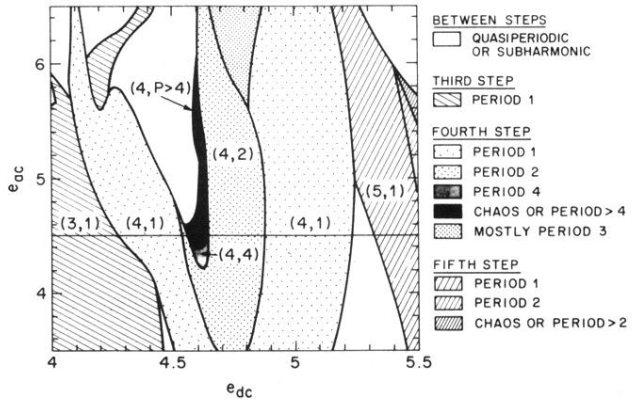

FIG. 4. A schematic picture of the solutions that are found in the e_{dc}-e_{ac} plane of Fig. 3. Harmonically mode-locked solutions are characterized by an index pair (n,P) which represents their entrainment n and periodicity P. (Boundaries between different regions are only approximate.) The horizontal line represents the intersection of parameter planes in Fig. 3.

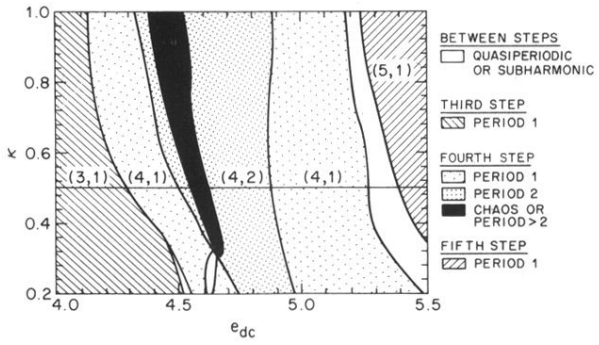

FIG. 7. Solutions in the e_{dc}-κ plane of Fig. 3. The horizontal line marks the intersection with the e_{dc}-e_{ac} plane of Fig. 4.